ResearchGate

See discussions, stats, and author profiles for this publication at: https://www.researchgate.net/publication/228456826

Secondary Crystallization Behavior of Poly(ethylene isophthalate- c o -terephthalate): Time-Resolved Small-Angle X-ray Scattering and Calorimetry Studies

ARTICLE *in* MACROMOLECULES · JUNE 2004

Impact Factor: 5.8 · DOI: 10.1021/ma0357321

CITATIONS
43

READS
43

6 AUTHORS, INCLUDING:

Byeongdu Lee
Argonne National Laboratory
205 PUBLICATIONS **6,479** CITATIONS
SEE PROFILE

Tae Joo Shin
Ulsan National Institute of Science and Tech…
127 PUBLICATIONS **2,604** CITATIONS
SEE PROFILE

Seung Woo Lee
Yeungnam University
208 PUBLICATIONS **3,995** CITATIONS
SEE PROFILE

Jinhwan Yoon
Dong-A University
47 PUBLICATIONS **1,696** CITATIONS
SEE PROFILE

Available from: Byeongdu Lee
Retrieved on: 26 January 2016

Secondary Crystallization Behavior of Poly(ethylene isophthalate-*co*-terephthalate): Time-Resolved Small-Angle X-ray Scattering and Calorimetry Studies

Byeongdu Lee, Tae Joo Shin, Seung Woo Lee, Jinhwan Yoon, Jehan Kim, and Moonhor Ree*

Pohang Accelerator Laboratory, Polymer Research Institute, Department of Chemistry, Center for Integrated Molecular Systems, Division of Molecular and Life Sciences, and BK21 Program, Pohang University of Science and Technology, San 31, Hyoja-dong, Pohang 790-784, Republic of Korea

Received November 18, 2003; Revised Manuscript Received February 11, 2004

ABSTRACT: Time-resolved small-angle X-ray scattering (SAXS) and differential scanning calorimetry (DSC) analyses were used to study the isothermal crystallization and remelting of poly(ethylene isophthalate-*co*-terephthalate)s containing 0−10 mol % isophthalate unit. For each of the polymers considered, evidence of the formation of both primary and secondary crystals was found in the SAXS pattern and its invariant *Q*, as well as in the DSC thermogram, which showed multiple melting endotherms. The melting of secondary crystals was found to shift significantly toward the high-temperature region with increasing crystallization time, indicating that the secondary crystals become thick and perfect over time. The thickness of the lamellar crystals was found to be very sensitive to the crystallization temperature, but no thickening was observed throughout the entire crystallization run, regardless of composition. The formation of secondary crystals, which favorably occurs during the later stages of crystallization, was found to cause a peak shift and an intensity increase in the SAXS pattern, a decrease in the SAXS invariant *Q*, and a decrease in the thickness of the amorphous layers in the lamellar stacks formed during primary crystallization. However, formation of secondary crystals was found not to be properly accounted for in the determination of the lamellar thickness from the SAXS patterns. The present results indicate that the secondary crystallization causes densification and shrinkage of the amorphous layers and that the resulting secondary crystals have lower electron density than the primary crystals. On the basis of the present results, we propose that secondary crystallization involves the formation of *short-range molecular order* in the amorphous layers of the lamellar stacks as well as in the amorphous regions between the lamellar stacks. This *short-range ordered structure*, which is likely a type of single thin lamella, thin lamellae, or fringed micelle-like order, has a lower electron density than the lamellar crystal formed by primary crystallization.

Introduction

Poly(ethylene terephthalate) (PET) is a representative semicrystalline polymer that is widely used as an engineering plastic material. Research into the morphology of semicrystalline polymers has utilized crystallization behavior as the key to understanding structure. The primary crystallization of PET has been studied in detail using various analytical techniques, including differential scanning calorimetry (DSC), small- and wide-angle X-ray scattering (SAXS and WAXS), small-angle light scattering, electron diffraction, transmission electron microscopy (TEM), atomic force microscopy (AFM), and infrared and Raman spectroscopy.[1−9] These studies have generated an extensive body of data related to the primary crystallization process.

Among the analytical techniques used to date, SAXS has been widely employed to investigate the morphology of PET after primary crystallization from the melt because it is the only conventional technique capable of probing the microstructure in real time. However, mathematical modeling is required to extract morphological parameters related to the semicrystalline structure from SAXS data. In general, adopting the simplest one-dimensional model consisting of alternating lamellar crystalline and amorphous layers (the infinite stack model), the SAXS data of PET have been analyzed by their inverse-cosine Fourier transformation to one-dimensional correlation function.[5,6] This type of correlation function analysis yields the first long period L as well as the thickness of one layer l_1 among the lamellar crystal and amorphous layers, according to Babinet's reciprocity theorem. As a result of this ambiguity in the SAXS analysis, the morphological assignments of l_1 and l_2 ($= L - l_1$) have been controversial.[5,6] Recently, this issue was resolved by a comprehensive analysis of SAXS data measured from PET and its random copolymers containing isophthalate units,[7] which indicated that the smaller thickness, l_1, corresponds to the lamellar crystal thickness, d_c, and that the larger thickness, l_2, corresponds to the amorphous layer thickness, d_a. This conclusion was consistent with AFM studies.[8]

Another approach that has been widely used to elucidate PET morphology has been to study the melting behavior of isothermally crystallized PET using DSC.[10−19] The resulting thermograms typically showed one to three endotherms, depending on the thermal history (i.e., crystallization temperature, crystallization time, and heating rate) of the sample, and the assignment of these endotherms remains a matter of controversy.[10−19] Although the factors underlying the appearance of multiple endotherms for PET are not fully understood, the observation of multiple endotherms suggests that, in the crystallization of PET, secondary crystallizations take place in addition to the primary crystallization.

* To whom all correspondence should be addressed: Tel +82-54-279-2120; Fax +82-54-279-3399; e-mail ree@postech.edu.

10.1021/ma0357321 CCC: $27.50 © 2004 American Chemical Society
Published on Web 04/30/2004

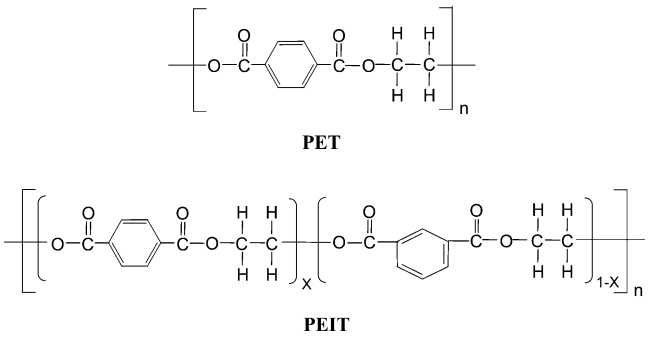

Figure 1. Chemical structures of poly(ethylene terephthalate) (PET) and its copolymer, poly(ethylene isophthalate-*co*-terephthalate) (PEIT).

The secondary crystallization behavior of PET has been scrutinized using SAXS, DSC, and microscopy.[4,5,18,20−23] As a result, three models have been proposed that take into account the secondary crystallization.[18,20−23] The first model involves the insertion of single lamella into the interlamellar region,[20−22] the second model involves the insertion of thin lamellar stacks between the stacks of lamellar crystals formed in the primary crystallization,[18] and the third model involves the formation of positive edge-on branched lamellar stacks.[23] However, there are still debated the merits of these models for the secondary crystallization of PET.

In contrast to PET, poly(ethylene isophthalate-*co*-terephthalate) (PEIT), a copolymer of PET, has been rarely studied by DSC[4,24] or SAXS.[25] Moreover, the one SAXS study of PEIT examined the crystallization of fiber-formed PEIT specimens rather than the crystallization of PEIT from the melt.[25]

Therefore, to better understand the secondary crystallization behavior of PET and its copolymer PEIT, we conducted detailed SAXS and DSC studies on the crystallization of the PET homopolymer and PEIT copolymers containing 4.9 and 9.8 mol % isophthalate (IPT) unit. In addition, we carried out a comprehensive analysis of the SAXS and DSC data and proposed a new structural model that can explain the crystallization of PET and PEIT.

Experimental Section

Polymer Sample Preparation. PET homopolymer and PEIT copolymers (chemical structures given in Figure 1) were synthesized by bulk polycondensation of the respective monomers, as described elsewhere;[4] here, the PEIT copolymers containing 4.9 and 9.8 mol % IPT unit are referred to as 5IPT and 10IPT, respectively. Both 5IPT and 10IPT have been previously studied to be random copolymers revealing single glass transition temperature T_g as well as single melting point T_m.[4] The minor component IPT unit in these copolymers has been known to play as a noncrystallizable unit.[4,7] The weight-average molecular weight $\overline{M}_w$ was 36 000 for PET, 37 000 for 5IPT, and 36 000 for 10IPT. The T_g and T_m were 76.1 and 258.6 °C for PET, 74.6 and 244.8 °C for 5IPT, and 73.5 and 234.2 °C for 10IPT, respectively.[4] The equilibrium melting temperature T_m^o was 275.4 °C for PET, 266.5 °C for 5IPT, and 261.9 °C for 10IPT.[4] The polymers were melt-molded under compression in a nitrogen atmosphere and cooled to room temperature, giving 2 mm thick sheets. These polymer sheets were cut either into disks of diameter 4 mm for use in X-ray scattering measurements or into tiny pieces for use in DSC measurements.

Measurements. SAXS measurements were conducted at the 4C1 SAXS beamline (BL)[26] of the Pohang Accelerator Laboratory at Pohang University of Science and Technology. In the 4C1 BL, a light source from a bending magnet of the PLS storage ring was focused by a toroidal silicon mirror coated with platinum and monochromatized with a W/B_4C double multiplayer monochromator, giving an X-ray beam of wavelength 1.608 Å. The X-ray beam size at the sample stage was 0.6 × 0.6 mm.[26] A one-dimensional silicon-photodiode array detector (model X/PDA-2048, Princeton Instruments) was employed. The distance between sample and detector was 1.0 m. The scattering angle was calibrated with linear polyethylene and collagen (chicken tendon) standards. SAXS measurements were carried out during isothermal crystallization of the polymer samples over 170−240 °C and then continued during subsequent remelting of the crystallized samples with a heating rate of 3.0 °C/min. Each measurement was collected for 10 s, with an average count per pixel of about 1200. In the measurements, a jumping hot stage consisting of two independent chambers under a nitrogen atmosphere was employed, and the temperatures of the chambers as well as the polymer sample were individually controlled and monitored by Eurotherm controllers with a K-type thermocouple. Each sample was first melted for 5 min in the top chamber and then quickly jumped to the bottom chamber, which was held at the chosen crystallization temperature T_c. Each SAXS intensity profile measured was normalized to the incident X-ray beam intensity, which was monitored by an ionization chamber placed in front of the sample and corrected further for the background run.

The measured SAXS profile was nonlinear-least-squares fitted with Porod's law:[27,28]

$$\lim_{q\to\infty} I(q) = I_b + \frac{K_p}{q^4} e^{-\sigma^2 q^2} \tag{1}$$

where $I(q)$ is the scattered intensity profile, I_b is the constant scattering from density fluctuations, σ is related to the interfacial thickness between the lamellar crystal and amorphous layer, and K_p is the Porod constant. Here, q is given by $q = (4\pi/\lambda) \sin\theta$, where λ is the wavelength of the X-ray source and 2θ is the scattering angle. The SAXS profile was then extrapolated to $q = 4$ nm^{-1} and the determined I_b was subtracted, after which the profile was corrected by multiplying by q^2, giving the Lorentz-corrected SAXS profile.

The Lorentz-corrected SAXS profile was inverse-cosine Fourier transformed to a one-dimensional correlation function $\gamma_1(z)$ in order to determine morphological parameters:[29−31]

$$\gamma_1(z) = \int_0^\infty q^2 I(q) \cos(qz)\, dq \tag{2}$$

where z is the direction normal to the layer faces in the stack. The one layer thickness l_1 in the lamellar crystal and amorphous layer stack was determined from the linear fit of the first decay slope in the plot of $\gamma_1(z)/\gamma_1(0)$ vs z. The long period L was obtained from the first peak maximum (z_{max}) of the same plot. The invariant Q was also determined from the Lorentz-corrected SAXS profile by the following equation:[20,27,29]

$$Q = \int_0^\infty q^2 I(q)\, dq \tag{3}$$

In addition, DSC thermograms were measured using a Seiko calorimeter calibrated with indium and tin standards. In the DSC measurements, all polymer samples were first melted and then jumped to the chosen crystallization temperature T_c, at which they underwent isothermal crystallization, followed by remelting at a heating rate of 3.0 °C/min, as described above for SAXS measurements. All measurements were made under a nitrogen atmosphere.

Results

Isothermal Crystallization−SAXS Analysis. Figures 2 and 3 show typical time-resolved SAXS patterns measured from PET and 5IPT polymers undergoing isothermal crystallization at the chosen temperatures,

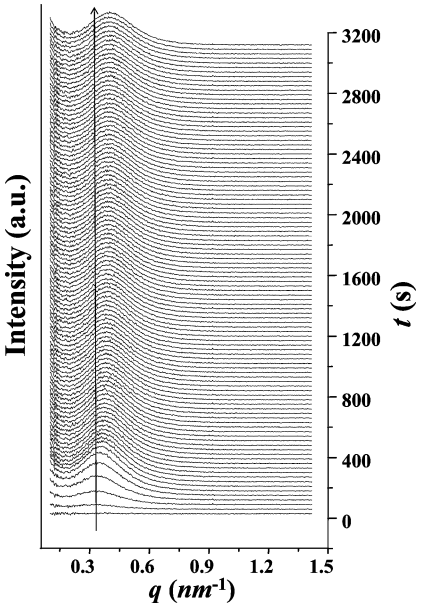

Figure 2. Time-resolved SAXS patterns of PET polymer measured during isothermal crystallization at 230 °C for 60 min.

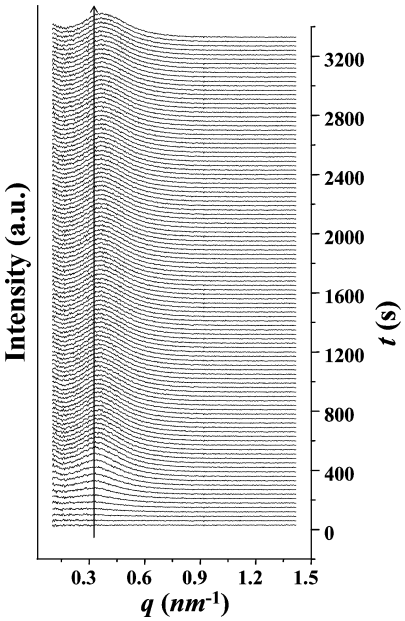

Figure 3. Time-resolved SAXS patterns of 5IPT copolymer measured during isothermal crystallization at 216 °C for 60 min.

respectively. As seen in the figures, the SAXS pattern is not detected initially in all the crystallization cases but develops with the structural evolution associated with crystallization. With increasing crystallization time the SAXS peak increases in intensity, and its maximum shifts to the high q region, finally remaining unchanged with further increase of the crystallization time.

The PEIT random copolymers 5IPT and 10IPT, which exhibited melting temperatures lower than that of the PET homopolymer, both always showed larger values of L and l_2 ($= L - l_1$) than those of the PET homopolymer. On the basis of these results, we can make the assignments $l_1 = d_c$ (lamellar crystal thickness) and $l_2 = d_a$ (interlamellar amorphous layer thickness). Figure 4 shows the variations in L, d_c, and d_a as a function of crystallization time and temperature for the PET homopolymer, and Figure 5 shows the corresponding data for 5IPT. For both PET and 5IPT, the lamellar crystal thickness d_c varies very little with time for the crystallization, indicating that no thickening occurred during the isothermal crystallization. In contrast, both L and d_a decreased during the isothermal crystallization over

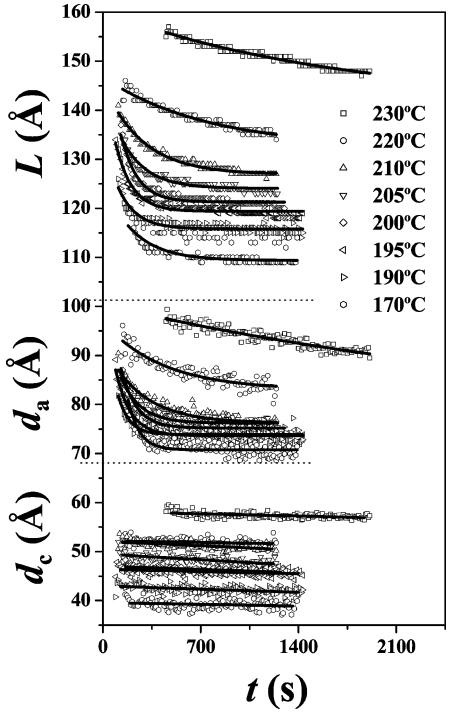

Figure 4. Variations of morphological parameters (long period L, amorphous layer thickness d_a, and lamellar crystal thickness d_c) with time obtained from the time-resolved SAXS patterns measured during isothermal crystallization of PET at various temperatures.

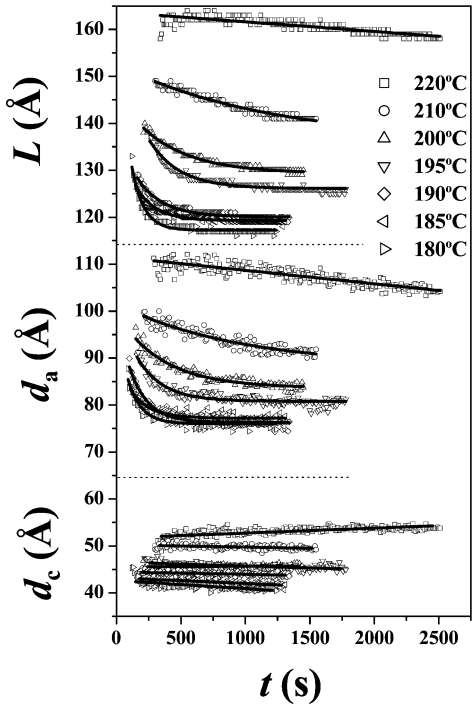

Figure 5. Variations of morphological parameters (long period L, amorphous layer thickness d_a, and lamellar crystal thickness d_c) with time obtained from the time-resolved SAXS patterns measured during isothermal crystallization of a PEIT copolymer, 5IPT, at various temperatures.

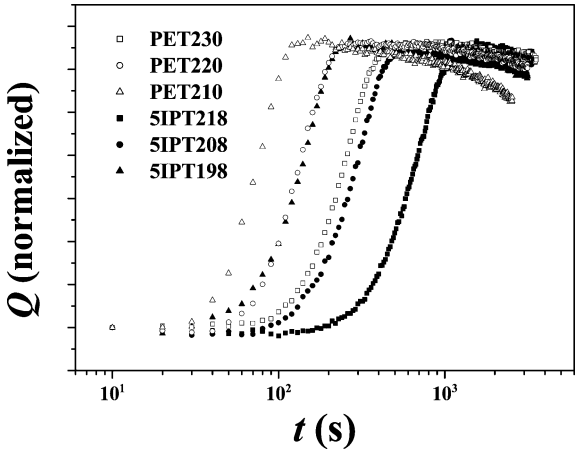

Figure 6. Time dependence of invariant *Q*'s obtained from SAXS patterns measured during isothermal crystallizations of PET polymer and 5IPT copolymer at various temperatures. The notation used indicates the polymer and its crystallization temperature: for example, PET230 refers to PET crystallized at 230 °C. The variation of *Q* with time at each crystallization temperature was were normalized by its maximum value.

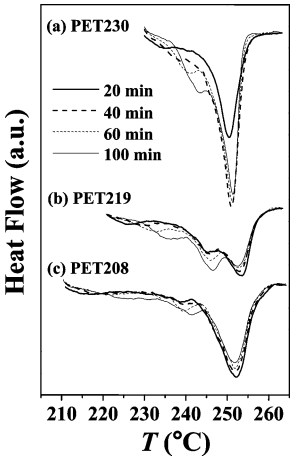

Figure 7. DSC thermograms of PET polymer crystallized isothermally for 20−100 min at various temperatures. The notation used indicates the polymer and its crystallization temperature: for example, PET230 refers to PET polymer crystallized at 230 °C. The heating rate used in the measurements was 3.0 °C/min.

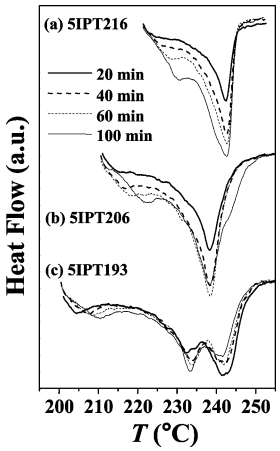

Figure 8. DSC thermograms of 5IPT polymer crystallized isothermally for 20−100 min at various temperatures. The notation used indicates the polymer and its crystallization temperature: for example, 5IPT216 refers to 5IPT polymer crystallized at 230 °C. The heating rate used in the measurements was 3.0 °C/min.

the temperature range considered. Similar trends were observed in the variations of L, d_c, and d_a for the 10IPT copolymer (data not shown). Given that d_c remained almost constant during the crystallization process, the reduction of L as crystallization proceeded can be seen as originating from the decrease of d_a.

The change in the invariant Q with crystallization time was determined from the SAXS patterns measured during isothermal crystallization. A selection of the Q values obtained from PET and 5IPT are presented in Figure 6. In the results presented here, the value of Q is normalized by its maximum value. For PET, the value of Q is small and constant for an initial induction period then increases rapidly with time up to a maximum at $t_{Q_{max}}$, after which it decreases slowly; here, $t_{Q_{max}}$ is the time at which the invariant Q reaches its maximum in the crystallization. Similar Q variations are observed for the 5IPT and 10PIT copolymers.

Remelting after Isothermal Crystallization—DSC and SAXS Analysis. The DSC thermograms, some of which are shown in Figures 7 and 8, were measured during the heating at 3.0 °C/min after isothermal crystallization for certain time. Both PET and its copolymers reveal multiple melting peaks, regardless of the crystallization conditions, as frequently observed for PET.[4,5,10−19]

As shown in Figure 7a, the PET sample crystallized at 230 °C displays two major melting peaks: one peak in the high-temperature region with a very large heat of melting and another peak in the low-temperature region. In general, lamellar crystals formed by primary crystallization are larger than those formed by secondary crystallization, causing them to melt in the high-temperature region. Thus, the peak in the high-temperature region can be assigned to the melting of crystals formed by primary crystallization. However, this melting endotherm may overlap either in part or fully with the exothermic peak of the recrystallization that can occur during heating.[11−14] The melting peak becomes more intense with increasing crystallization time, whereas the peak position varies very little with time. This behavior suggests that the crystals grow via crystallization, but they thicken very little. The peak in the low-temperature region is assigned to the melting of the crystals formed by secondary crystallization. This peak is initially very weak but increases in intensity with time. Furthermore, the peak shifts substantially to the high-temperature region with increasing crystallization time. These results suggest that, at later times in the isothermal crystallization, new crystals form in a secondary process and undergo growth and thickening. Similar melting behavior is observed for the 5IPT sample crystallized at 216 °C (see Figure 8a).

Different from the results presented above, the PET sample crystallized at 219 °C shows three major melting peaks (see Figure 7b). This sample exhibits two melting peaks in the high-temperature region, rather than the single melting peak seen for PET crystallized at 230 °C. The peaks in the high-temperature region appear at around 247 and 253 °C, which fall either side of the peak due to the lamellar crystals formed by primary crystallization at 230 °C. It is well-known that thinner lamellar crystals form at lower crystallization temperatures and that these crystals exhibit low melting points. We therefore assign the peak at around 247 °C to the melting of the lamellar crystals formed by the primary crystallization, and the peak at around 253 °C is

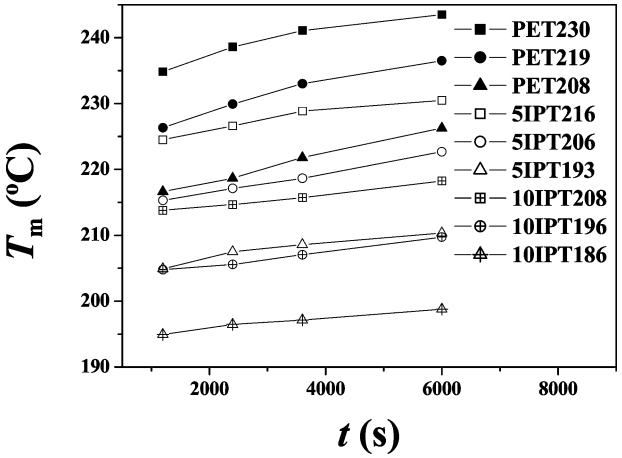

Figure 9. Variation of T_m (the melting point of secondary crystals) with crystallization time in PET polymer and its copolymers (5IPT and 10IPT) crystallized isothermally at various temperatures. Here, T_m was estimated from the peak maximum of the melting in the lowest temperature region in the DSC measurement. The notation used indicates the polymer and its crystallization temperature: for example, PET230 refers to PET polymer crystallized at 230 °C.

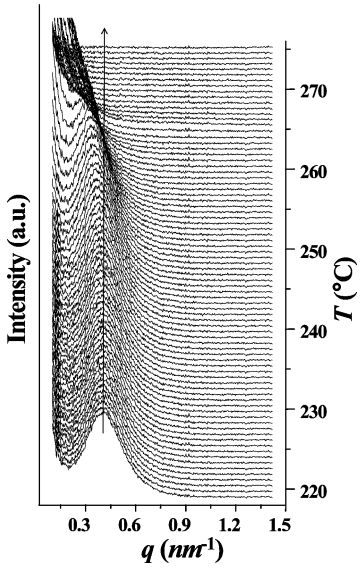

Figure 10. Time-resolved SAXS patterns of PET polymer measured during subsequent heating at 3.0 °C/min after isothermal crystallization at 230 °C for 60 min.

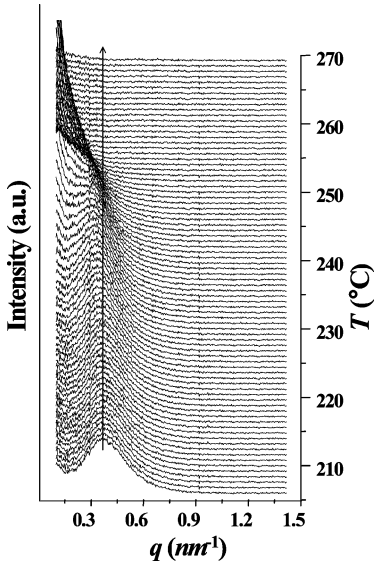

Figure 11. Time-resolved SAXS patterns of 5IPT polymer measured during subsequent heating at 3.0 °C/min after isothermal crystallization at 230 °C for 60 min.

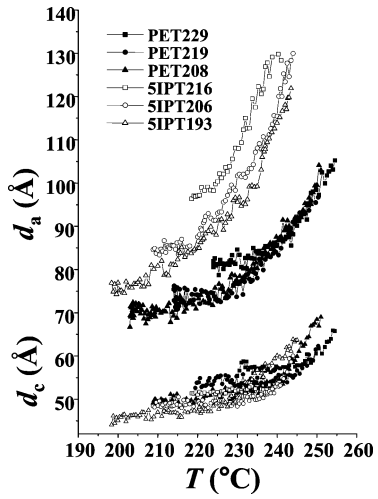

Figure 12. Variation of amorphous layer thickness d_a and lamellar crystal thickness d_c with temperature estimated from the SAXS patterns measured during subsequent heating at 3.0 °C/min after isothermal crystallization of PET polymer and 5IPT copolymer for 60 min at various temperatures. The notation used indicates the polymer and its crystallization temperature: for example, PET230 refers to PET polymer crystallized at 230 °C.

assigned to the melting of crystals that recrystallized during the heating run. The melting point of the crystals from the secondary crystallization, and its shift with crystallization time, are also detected in this sample. The PET sample crystallized at 208 °C shows similar behavior to that described above (see Figure 7c), as do the 5IPT and 10IPT samples crystallized over 190−210 °C (see Figure 8b,c).

From the DSC results presented above, we find that the multiple melting endotherms in the isothermally crystallized PET and its copolymers originate from the melting of the crystals formed by primary and secondary crystallization. In addition, it is noteworthy that the melting point of the recrystallized crystals is observed for PET, and its copolymers crystallized at relatively high degrees of supercooling.

For crystals formed by primary crystallization at a particular temperature, the melting endotherm peak increases in intensity with increasing crystallization time, whereas the position of its maximum (i.e., melting point) does not vary with time. This behavior, which was found for both the homopolymer and copolymers, suggests that the size (i.e., crystal thickness) of crystals formed by primary crystallization does not vary substantially with time during isothermal crystallization. This is consistent with the SAXS results discussed in the earlier section (see Figures 4 and 5).

In Figure 9, the melting points of the crystals formed by secondary crystallization are plotted as a function of crystallization time for a range of systems. The results clearly show that longer crystallization times generate secondary crystals with higher melting points. This suggests that over time the crystals that are formed by secondary crystallization become thick and perfect, and their population increases. In addition, the rate of

increase of the melting point in the secondary crystals is more rapid in the PET polymer than in the copolymers. This suggests that the thickening and perfectioning of crystals formed by secondary crystallization, and their population growth, take place more rapidly in the PET polymer than in the copolymers. Consequently, secondary crystallization causes specimens of PET and its copolymers to undergo densification.

As discussed with the DSC results (Figures 7 and 8) above, 60 min was found to be sufficient for both primary and secondary crystallization to occur. To further investigate the melting behavior of PET and its copolymers, SAXS and DSC measurements were therefore conducted during the heating run at a rate of 3.0 °C/min after isothermal crystallization for 60 min at a temperature in the range 190−230 °C.

Figures 10 and 11 show typical time-resolved SAXS patterns of PET and 5IPT polymers measured during remelting after isothermal crystallizations at 230 and 216 °C, respectively. As seen in the figures, with increasing temperature the SAXS pattern weakens in intensity and shifts its peak maximum to the low-q region, finally disappearing. From these SAXS patterns measured during the remelting of isothermally crystallized PET and its copolymers, the morphological parameters have been extracted. Figure 12 presents the temperature dependence of the lamellar crystal and amorphous layer thicknesses for PET and 5IPT under all of the crystallization conditions studied. During heating runs of PET and its copolymers, their lamellar crystal thickness d_c very slowly increases with temperature up to around 240 °C and thereafter turns to increase rapidly. However, the amorphous layer thickness d_a of PET always rapidly increases with temperature, compared to the lamellar crystal thickness d_c. In the heating run of the copolymers, the amorphous layer thickness d_a more rapidly increases with temperature compared to that of PET. These temperature dependences of the morphological parameters will be further discussed below, with taking into consideration DSC data of isothermally crystallized PET and its copolymers. Figure 12 additionally shows the following interesting features. For PET polymer, the temperature dependence of d_a is independent of crystallization temperature, within a small fluctuation level. A similar trend is observed for 5IPT copolymer isothermally crystallized at 193 and 206 °C. However, the variation of d_a with temperature in 5IPT crystallized at 216 °C deviates slightly from the behavior observed at the two lower crystallization temperatures. The temperature dependence of the lamellar crystal thickness d_c, on the other hand, shows the same basic behavior for all crystallization temperatures and polymer compositions.

Figure 13 shows SAXS morphological parameters plotted together with DSC thermograms, which were measured during remelting of the isothermally crystallized PET and 5IPT. As seen in the figure, in the heating run, the value of d_c varies very little with temperature through the melting of the crystals formed by secondary crystallization and continues to show little variation up to the temperature of the peak maximum corresponding to the melting of lamellar crystals formed during primary crystallization. This behavior was observed regardless of polymer composition and crystallization temperature. At higher temperatures d_c increases rapidly with increasing temperature through the meltings of the crystals formed during primary crystallization and the recrystallized crystals. The increase of d_c with temperature is particularly marked through the melting of the crystals formed by recrystallization during the heating run. This behavior is detected in samples crystallized with high degrees of supercooling. In contrast, the value of d_a initially increases slowly with temperature. With further increase of the temperature the increase in d_a becomes steeper. This behavior is observed regardless of polymer composition and crystallization temperature. Actually, increase of d_a can be caused by the thermal expansion and melting of thinner lamellae (i.e., secondary crystals) between thicker lamellae (i.e., primary crystals). Slower increase at lower temperature is mainly from the former reason, and faster increase can be from both reasons.

Remelting of Secondary Crystals—SAXS Analysis. Figure 14 shows SAXS patterns measured at the melting point of the secondary crystals in the heating run after isothermal crystallization, which are compared to those measured at $t = (t_{Q_{max}} + 100\ s)$ and $t = 3600$ s in the crystallization run. In the results presented here, $t_{Q_{max}}$ is taken as the crossover time between primary and secondary crystallization. In this scheme, primary crystallization predominates up to this time, and thereafter secondary crystallization occurs to a greater extent. As shown in Figure 14a, for the PET crystallized at 230 °C, the SAXS pattern measured at $t = 3600$ s appears in the high-q region and with a low intensity in comparison to that measured at $t = 500$ s [$= (t_{Q_{max}} + 100)$ s]. Taking the DSC result of Figure 13a into account, the position shift to the high-q region and the intensity reduction in the SAXS pattern due to the longer crystallization are attributed to the formation of secondary crystals. On the other hand, in the subsequent heating run the SAXS pattern measured at 245 °C is exactly the same as that measured at $t = 500$ s. Taking the DSC result of Figure 13a into account, the position shift to the low-q region and the intensity increase in the SAXS pattern due to the subsequent heating originate from the remelting of secondary crystals formed during the crystallization run. Similar results are observed for PET, and its copolymers crystallized at other temperatures (see Figure 14b−d). Overall, these SAXS measurements clearly demonstrate that the formation of secondary crystals and their melting cause a peak shift and an intensity change in the SAXS pattern. These results highlight the power of the SAXS technique as a tool for sensitively monitoring secondary crystallization in PET and its copolymers. Conclusively, these SAXS results indicate that both secondary and primary crystals form during the crystallization of PET and its copolymers and that, if the crystallized polymer is heated, the secondary crystals melt before the primary crystals.

Discussion

Here we consider three morphological models[18,20−23] that were proposed for the morphological structure of PET created by secondary crystallization in addition to primary crystallization and then evaluate their validity for the secondary crystallization of PET and its copolymers investigated in the present study.

The single thin lamellar insertion model[20−22] assumes the following: (1) secondary crystallization generates single thin lamellae in the amorphous layers of the lamellar stacks formed during primary crystallization, and (2) the thicknesses of the lamellar and amorphous

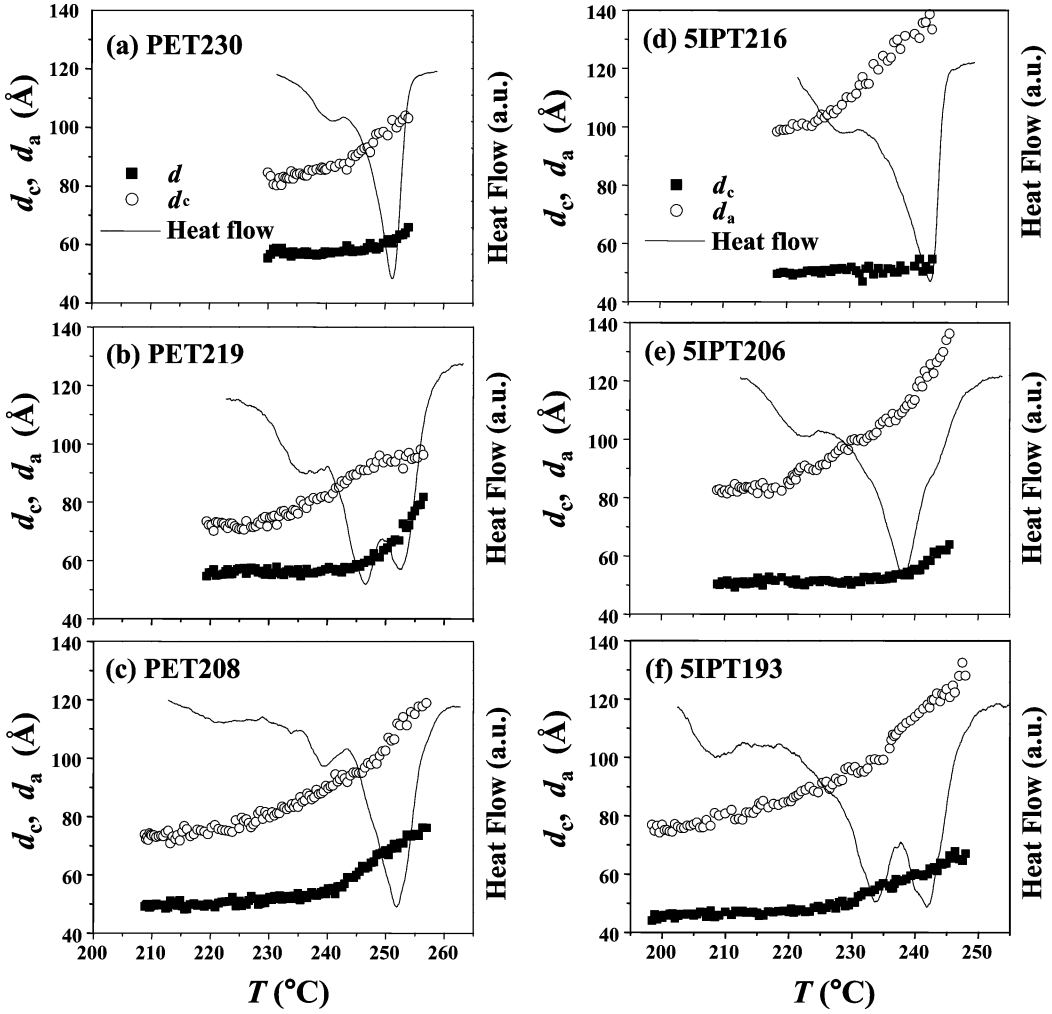

Figure 13. DSC thermograms, as well as variations of amorphous layer thickness d_a and lamellar crystal thickness d_c with temperature, measured during heating at 3.0 °C/min after isothermal crystallization of PET polymer and 5IPT copolymer for 60 min at various temperatures. The notation used indicates the polymer and its crystallization temperature: for example, PET230 refers to PET polymer crystallized at 230 °C.

layers in the lamellar stack formed during primary crystallization remain constant throughout the secondary crystallization process. Thus, the overall crystallinity should increase as the secondary crystallization proceeds. The invariant Q of the SAXS profile always increases throughout entire crystallization. The rate of increase in the invariant Q depends on the population of single thin lamellae. Because of the insertion of single thin lamellae, the long period in the lamellar stacks formed during primary crystallization decreases by 50% as the secondary crystallization proceeds. The amorphous layer thickness in the lamellar stacks formed during primary crystallization also decreases with time by more than 50% during the secondary crystallization. This reduction in the thickness of the amorphous layers, and the consequent reduction in the long period, cause the SAXS peak to shift substantially toward the high-q region. In the model, the electron density of the single thin lamellae formed during secondary crystallization was not clearly described but generally considered accountable enough to contribute to the SAXS pattern; in the extreme case, single thin lamellae would have the same electron density as the lamellar crystals formed during primary crystallization.[20−22] Thus, taking the electron density into account, the lamellar layer thickness would be expected to decrease somewhat if a reasonably high population of single thin lamellae were to form. This reduction in lamellar layer thickness would make a positive contribution to the shift of the SAXS peak to the high-q region.

The thin lamellar stack insertion model[18] involves the following assumptions: (1) the secondary crystallization process involves the formation of thin lamellar stacks among the lamellar stacks already formed during primary crystallization, (2) the amorphous layer thickness in the lamellar stacks formed during primary crystallization is constant throughout the entire crystallization process, (3) the amorphous layer thickness in the thin lamellar stacks formed during secondary crystallization is the same as that in the lamellar stacks formed during primary crystallization, and (4) the lamellar thickness in the lamellar stacks formed during secondary crystallization is smaller than that of the lamellar stacks formed during primary crystallization. Thus, the overall lamellar thickness decreases with time when secondary crystallization takes place, which means that the thinning of the overall lamellar thickness occurs throughout the entire crystallization process. In addition, the formation of thin lamellar stacks should cause the SAXS profile to broaden and shift to the high-q region as crystallization proceeds. In the extreme case that these thin lamellar stacks form in a reasonably high population, the SAXS profile may appear to have two peaks. Finally, the overall crystallinity increases

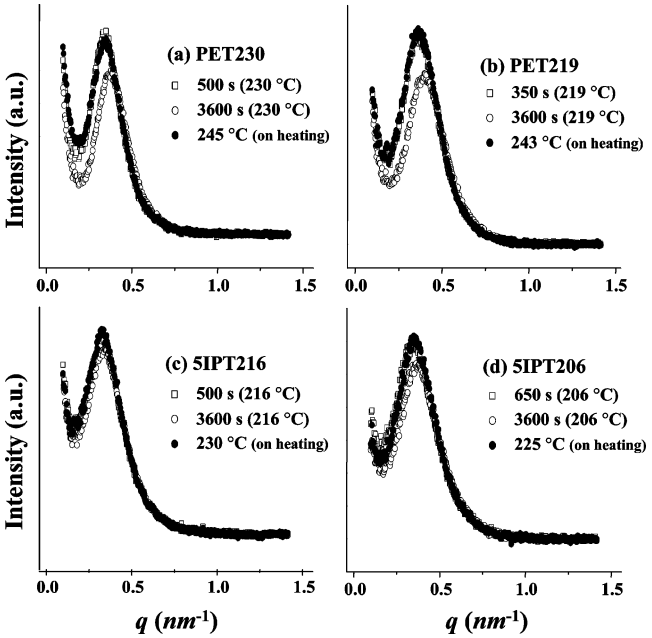

Figure 14. SAXS patterns measured during isothermal crystallization and subsequent heating of PET and 5IPT polymers: □, measured at $t = (t_{Q_{max}} + 100$ s) in the crystallization of the polymer at the chosen temperature; ○, measured at $t = 3600$ s in the crystallization of the polymer at the chosen temperature; ●, measured at a certain temperature (namely, the melting temperature of secondarily crystallized crystals or just above) on the subsequent heating run at 3.00 °C/min after crystallizing for $t = 3600$ s at the chosen temperature. Here, $t_{Q_{max}}$ is the time at which the invariant Q of the SAXS pattern reaches its maximum in the crystallization.

continuously due to the formation of the thin lamellar stacks by secondary crystallization. Thus, the invariant Q should always increase throughout the entire crystallization process.

The positive edge-on branched lamellar stack model,[23] on the other hand, assumes the following: (1) the secondary crystallization process involves the formation of secondary crystals along the edges of the lamellae formed during primary crystallization, and (2) the thicknesses of the lamellar and amorphous layers in the lamellar stack formed during primary crystallization remain constant throughout the secondary crystallization process. Thus, the lamellar thickness apparently increases with time when secondary crystallization occurs, which causes an increase of optical retardation.[23] On the contrary, the optical retardation on melting decreases due to a reduction in the apparent lamellar thickness at constant birefringence.[23] The SAXS profile would have two types of long period: one originates from the stack of lamellae formed by primary crystallization and the other from the secondary lamellar stacks branched on edges of the lamellae formed by primary crystallization. Further, both primary and secondary lamellar crystal thicknesses would be detectable in the SAXS analysis.[23] Finally, the overall crystallinity increases continuously due to the formation of the positive edge-on branched lamellar stacks by secondary crystallization. Thus, the invariant Q should always increase throughout the entire crystallization process.

However, the SAXS profiles, Q variations, long periods, lamellar crystal thicknesses, amorphous layer thicknesses, and DSC melting endotherms found in the present study are quite different from those predicted by the above three models.

First, the lamellar crystal thickness d_c was found to vary very little during the entire crystallization process, even including the later stages of crystallization (see Figures 4 and 5). This result is a significant departure from those predicted by the thin lamellar stack insertion model and the positive edge-on branched lamellar stack model. In subsequent remelting after the isothermal crystallization of PET and its copolymers, the lamellar thickness d_c also varies very little through the melting of the secondary crystals and continues to show little variation up to the temperature of the DSC endotherm peak maximum corresponding to the melting of primary lamellar crystals (see Figure 13). These results are different from those predicted by the positive edge-on branched lamellar stack model. These results suggest that the secondary crystals in the isothermally crystallized polymers are not properly accounted for in the calculation of the lamellar thickness d_c from the SAXS patterns. This event only manifests when the secondary crystals are of much lower density than the primary lamellar crystals or when the secondary crystals are much thinner than the primary lamellar crystals. In the latter case, the thinner secondary crystals would only weakly contribute to the lamellar thickness d_c in the SAXS patterns, even though their electron density is the same as that of the primary lamellar crystals. As described above, the single thin lamellar insertion model predicts that the amorphous layer thickness in the lamellar stacks formed during primary crystallization will decrease by more than 50% during the secondary crystallization. However, no such large decrease of the amorphous layer thickness was observed during the secondary crystallization, suggesting that the secondary crystallization process in PET and its copolymers produces secondary crystals different from the single thin lamellae that are assumed to form under the single thin lamellar insertion model. Taking this into account, the present d_c results lead to the conclusion that, in the isothermal crystallizations of PET and its copolymers, the secondary crystals have relatively low electron density compared to that of the primary crystals, and hence the contribution of the secondary crystals to the lamellar thickness d_c determined from the SAXS pattern is very small.

Second, in contrast to the behavior of the lamellar crystal thickness d_c, the amorphous layer thickness d_a in PET and its copolymers was found to decrease during primary crystallization (see Figures 4 and 5). Various factors could potentially contribute to the observed decrease in d_a during primary crystallization, including (1) the distribution of d_a in the lamellar stacks and its variation with time, (2) the number of lamellae in the lamellar stacks and its effect on the SAXS profile, and (3) relaxation of the polymer chains in the amorphous layers. The amorphous layer thickness d_a further decreases during the secondary crystallization process, as shown in Figures 4 and 5. In contrast, during the subsequent remelting after the isothermal crystallization of PET and its copolymers, the amorphous layer thickness d_a increases during the melting of the secondary crystals and then increases more rapidly during the melting of the primary lamellar crystals (see Figure 13). Overall, the changes in d_a due to secondary crystallization as well as those due to remelting of the secondary crystals are less than 15% of the amorphous layer thickness in the lamellar crystal stack formed during primary crystallization; this finding is a significant

departure from the behavior predicted by the single thin lamellar insertion model.

Third, the long period L in the SAXS pattern was found to decrease during the entire crystallization (see Figures 3 and 4). However, the decrease in L is less than 15% with respect to the value of L in the lamellar stacks formed during primary crystallization (see Figures 3 and 4), which is much smaller than the large reduction (50% reduction) predicted by the single thin lamellar insertion model.

Fourth, the SAXS patterns do not show broadening as crystallization progresses (see Figures 2 and 3), which is a departure from the formation of two peaks or broadening in the SAXS pattern predicted by the thin lamellar stack insertion model and by the positive edge-on branched lamellar stack model. The peak maximum of the SAXS pattern was found to shift to the high-q region (see Figures 2, 3, and 14), but the extent of this peak shift was smaller than that predicted by the single thin lamellar insertion model. In addition, the intensity of the SAXS pattern clearly diminished during the secondary crystallization (see Figure 14). This intensity reduction in the SAXS pattern during secondary crystallization is the opposite of the behavior predicted by both the single thin lamellar insertion model and the thin lamellar stack insertion model. Taking this result into account, along with the behavior of d_c and d_a described above, the observed peak shift and intensity reduction in the SAXS pattern during the crystallization (Figures 2, 3, and 14) can be mainly attributed to the reduction of the amorphous layer thickness d_a due to the formation of secondary crystals that are different both from the single thin lamellae described by the single thin lamellar insertion model and from the thin lamellar stacks described by the thin lamellar stack insertion model.

Fifth, the single thin lamellar insertion model predicts the following four-stage variation of the amorphous layer thickness d_a during remelting of isothermally crystallized samples: (1) d_a increases slowly before the first melting endotherm [i.e., melting of single thin lamellae (secondary crystals)]; (2) during melting of the single thin lamellae, a steeper increase in d_a is expected; (3) between the first (melting of single thin lamellae) and second (remelting of primary lamellae) endotherms, the rate of increase of d_a would be reduced because there is only thermal expansion; and (4) d_a would be expected to increase fastest during the melting of the primary lamellae. However, this four-stage pattern was not observed for the PET and its copolymers examined in the present study (see Figure 13).

Sixth, the SAXS invariant Q, as seen in Figure 6, is small and constant for an initial induction period and then increases rapidly with time up to a maximum at $t_{Q_{max}}$, after which it decreases slowly. The decrease in Q during the later stages of crystallization (i.e., during secondary crystallization) is the opposite of the behavior predicted by the above three models. This finding provides further evidence that the secondary crystals formed in PET and its copolymers have a morphology different from those assumed by the three models.

To understand the observed behavior of the invariant Q, consider the relationship between the invariant Q and the morphological parameters of the polymer samples. For a pseudo-two-phase structure with a linear density gradient of interface between the crystal and amorphous layers, the invariant Q in eq 3 can be expressed by the following equation:[30−33]

$$Q = K\alpha_s\left[\varphi_c(1-\varphi_c) - \frac{\sigma O_s}{6}\right](\rho_c - \rho_a)^2 \qquad (4)$$

where K is a conversion constant between electron and macroscopic densities, α_s is the volume fraction of lamellar stacks within the total, irradiated sample volume, φ_c and $(1-\varphi_c)$ are the volume fractions of the crystalline and amorphous phases in the lamellar stacks, respectively, σ is the thickness of interface between the crystal and amorphous layers, O_s is the specific surface area of the phase boundary, and ρ_c and ρ_a are the temperature-dependent electron densities of the crystalline and amorphous phases, respectively.

The PET and its copolymer samples, which were isothermally crystallized for 60 min over 170−240 °C, reveal a heat of fusion (ΔH_f) ranging from 32.7 to 53.1 J/g, depending on the composition and crystallization temperature, in the heating run (see some DSC endotherms in Figures 7 and 8). The completely crystallized PET homopolymer was reported to have a heat of fusion of 117.6−140.3 J/g (=$\Delta H_f°$).[2,3] Using these $\Delta H_f°$ values, the bulk crystallinities (x_c) of the polymer samples are estimated to range from 23.3 to 45.1% from the measured ΔH_f values. The value of x_c is directly related to the φ_c in eq 4. During the crystallization, φ_c increases by less than 50%. Taking this fact into account, the term $[\varphi_c(1-\varphi_c)]$ in eq 4 does not decrease during crystallization. Furthermore, the parameter α_s in eq 4 would not decrease with time as crystallization progresses. These facts suggest that the decrease of Q at times greater than $t_{Q_{max}}$ (i.e., during secondary crystallization) results from the reduction of $(\rho_c - \rho_a)$, the difference between the electron densities of lamellar crystal layer ρ_c and amorphous layer ρ_a. As the value of ρ_c would not decrease with crystallization time, the decrease of the $(\rho_c - \rho_a)$ term is attributed to an increase in ρ_a, signifying a densification of the amorphous layers via secondary crystallization. This densification shrinks the amorphous layers, consequently reducing the amorphous layer thickness d_a. Such a shrinking of the amorphous layers was discussed above in regard to the variations of the morphological parameters with crystallization time, where it was found that d_a decreases but d_c does not vary during crystallization, regardless of the polymer composition (see Figures 4 and 5).

Finally, the DSC study in the present work found that longer crystallization times of PET as well as its copolymers generate secondary crystals with higher melting points (see Figures 7−9). These results indicate that over time the crystals that are formed by secondary crystallization become thick and perfect, and their population increases. Neither the single thin lamellar insertion model nor the thin lamellar stack insertion model can explain these results.

In summary, both the single thin lamellar insertion model and the thin lamellar stack insertion model are inappropriate to explain the morphological structures of PET and its copolymers crystallized from the melt in the present study.

Taking into account all the results presented above, we here propose a *new structural model* describing the amorphous layers in a lamellar stack and the amorphous regions between lamellar stacks, which become dense and shrink due to secondary crystallization. The proposed model involves a *short-range-ordered structure*

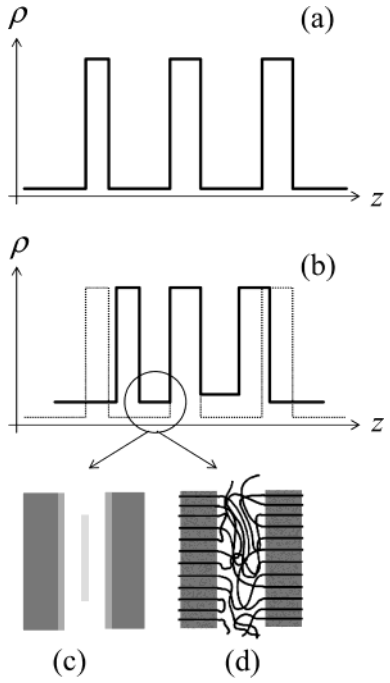

Figure 15. (a) Schematic electron density profile of a lamellar crystal stack along the direction normal to the lamellar crystal plane, which is formed by primary crystallization. (b) Electron density profile (solid line) of a lamellar crystal stack along the direction normal to the lamellar crystal plane, which is formed by secondary crystallization after primary crystallization: here, the broken line is the electron density profile of a primary lamellar crystal stack, which is same with that in (a). (c and d) Schematic pictures of single thin lamella and fringed micelle-like structure formed possibly in the amorphous layer by secondary crystallization, respectively. Such single thin lamella and fringed micelle-like structure also are possibly formed in amorphous regions between primary lamellar crystal stacks. Here, electron densities (ρ_{sros}) of both single thin lamella and fringed micelle-like structure should be limited to the range defined by eq 5.

that has a lower electron density than the lamellar crystals formed by primary crystallization. A schematic picture of the structural model is shown in Figure 15. The electron density (ρ_{sros}) of this *short-range-ordered structure* is allowed to vary over the range:

$$\rho_a < \rho_{sros} < |\langle\rho\rangle - \rho_a| + \langle\rho\rangle \qquad (5)$$

where $\langle\rho\rangle = \varphi_c\rho_c + (1 - \varphi_c)\rho_a$, φ_c and ρ_c are the volume fraction and electron density of lamellar crystals, respectively, and $(1 - \varphi_c)$ and ρ_a are the volume fraction and electron density of amorphous phases, in the lamellar stack formed by primary crystallization before the commencement of secondary crystallization. The *short-range-ordered structure* can consist of single thin lamella (see Figure 15c), thin lamellae, or fringed micelle-like molecular order (see Figure 15d), which must obey the electron density limit defined by eq 5.

A fringed micelle-like structure has been previously proposed for secondary crystals formed during the crystallizations of a poly(ether ether ketone)[34,35] and ethylene copolymers.[36] However, in all these studies the micelle-like morphology was suggested only on the basis of observation of multiple endotherms in DSC measurements, without any support from structural data.

Conclusions

The isothermal crystallization and remelting of PET and its copolymers containing 4.9 and 9.8 mol % IPT unit were investigated in detail using time-resolved SAXS and DSC. The PET and its copolymers exhibited several characteristic behaviors.

First, the formation of both primary and secondary crystals was evident from the variation of the SAXS pattern and invariant Q during the crystallization and subsequent remelting and also from the multiple endotherms exhibited by the isothermally crystallized samples.

Second, the thickness d_c of lamellar crystals (i.e., primary crystals) was very sensitive to the crystallization temperature, indicating that the degree of supercooling is the major driving force determining the thickness of lamellar crystals. However, no thickening was observed during the isothermal crystallization of any of the polymers considered. Instead, the lamellar crystal underwent perfectioning and lateral growth during the crystallization process, causing its melting temperature to increase slightly.

Third, the secondary crystals, which favorably form during the later stages of crystallization, become thick and perfect over time, and their population increases, causing the melting temperature of these crystals to increase significantly.

Fourth, the secondary crystals in the isothermally crystallized polymers are not properly accounted for in the calculation of the lamellar thickness d_c from the SAXS patterns, indicating that the secondary crystals have much lower electron density than the primary crystals.

Fifth, the formation of secondary crystals causes the peaks in the SAXS pattern to shift to higher q and an intensity reduction in the SAXS pattern with no broadening, whereas the melting of secondary crystals causes a peak shift to lower q and an intensity increase in the SAXS pattern with no broadening. These results indicate that the amorphous layers in the lamellar stack formed during primary crystallization shrink (i.e., increase in density) during secondary crystallization and then become less dense on melting of the secondary crystals.

Sixth, the amorphous layer thickness d_a decreases during the overall crystallization (i.e., primary and secondary crystallization). Several factors potentially contribute to the decrease in d_a during the primary crystallization, including (1) the d_a distribution in lamellar stacks and its variation with time, (2) the number of lamellae in the lamellar stacks and its effect on the SAXS profile, and (3) relaxation of polymer chains in the amorphous layers. On the other hand, the decrease in d_a during the secondary crystallization can be attributed to the formation of secondary crystals and their thickening and perfectioning in the amorphous layers in the lamellar stacks formed during primary crystallization and in the amorphous regions between the lamellar stacks.

Finally, the SAXS invariant Q is small and constant for an initial induction period and then increases rapidly with time up to a maximum at $t_{Q_{max}}$, after which it decreases slowly. The decrease in Q during the later stages of crystallization (i.e., during secondary crystallization) originates from the reduction of $(\rho_c - \rho_a)$, the difference between the electron densities of the lamellar crystal layer ρ_c and the amorphous layer ρ_a. The decrease of $(\rho_c - \rho_a)$ is attributed to an increase in ρ_a, signifying a densification of the amorphous layer via secondary crystallization.

Considering all these results, we propose a *new structural model* capable of describing the behavior of the amorphous layers in the lamellar stacks and the amorphous regions between the lamellar stacks in PET and its copolymers as they undergo secondary crystallization. The proposed model involves a *short-range-ordered structure* that has a lower electron density than the lamellar crystals formed by primary crystallization. The *short-range-ordered structure* may consist of single thin lamella, thin lamellae, or fringed micelle-like molecular order, which must obey the electron density limit outlined in the main text.

Acknowledgment. This study was supported by the Center for Integrated Molecular Systems (KOSEF). The synchrotron SAXS measurements were supported by MOST and POSCO.

References and Notes

(1) (a) Balta, F. J.; Santa Cruz, C.; Asano, T. *J. Polym. Sci.: Polym. Phys. Ed.* **1993**, *31*, 557. (b) Liu, J.; Geil, P. H. *J. Macromol. Sci., Phys.* **1997**, *36*, 61. (c) Lu, X.; Windle, A. H. *Polymer* **1996**, *37*, 2027. (d) Lindner, W. L. *Polymer* **1973**, *14*, 9. (e) Hachiboshi, M.; Fukuda, T.; Kobayashi, S. *J. Macromol. Sci., Phys.* **1969**, *3*, 525. (f) Lin, S.-B.; Koenig, J. L. *J. Polym. Sci.: Polym. Phys. Ed.* **1983**, *21*, 2365. (g) Yamashita, Y. *J. Polym. Sci., Part A* **1965**, *3*, 81. (h) Groeninckx, G.; Reynaers, H.; Berghmans, H.; Smets, G. *J. Polym. Sci.: Polym. Phys. Ed.* **1980**, *18*, 1331. (i) Chen, W.; Lofgren, E. A.; Jabarin, S. A. *J. Appl. Polym. Sci.* **1998**, *70*, 1965. (j) Everall, N.; Tayler, P.; Chalmers, J. M.; MacKerron, D.; Ferwerda, R.; van der Maas, J. H. *Polymer* **1994**, *35*, 3184.

(2) (a) Yamadera, R.; Murano, M. *J. Polym. Sci., Part A-1* **1967**, *5*, 2259. (b) Choe, C. R.; Lee, K. H. *Polym. Eng. Sci.* **1988**, *29*, 801. (c) Kitano, Y.; Kinoshita, Y.; Ashida, T. *Polymer* **1995**, *36*, 1947. (d) Fischer, E. W.; Fakirov, S. *J. Mater. Sci.* **1976**, *11*, 1041. (e) Wunderlich, B. *Polym. Eng. Sci.* **1978**, *18*, 431.

(3) (a) Lee, S. W.; Lee, B.; Ree, M. *Macromol. Phys. Chem.* **2000**, *201*, 453. (b) Yu, J.; Zhou, D.; Chai, W.; Lee, B.; Lee, S. W.; Yoon, J.; Ree, M. *Macromol. Res.* **2003**, *11*, 25.

(4) Lee, S. W.; Ree, M.; Park, C. E.; Jung, Y. K.; Park, C.-S.; Jin, Y. S.; Bae, D. C. *Polymer* **1999**, *40*, 7137.

(5) (a) Rule, R. J.; MacKerron, D. H.; Mahendrasingam, A.; Martin, C.; Nye, T. M. W. *Macromolecules* **1995**, *28*, 8517. (b) Koncke, U.; Zachmann, H. G.; Balta-Calleja, F. J. *Macromolecules* **1996**, *29*, 6019. (c) Lee, C. H.; Saito, H.; Inoue, T.; Nojima, S. *Macromolecules* **1996**, *29*, 7034. (d) Santa Cruz, C.; Stribeck, N.; Zachmann, H. G.; Balta Calleja, F. J. *Macromolecules* **1991**, *24*, 5980.

(6) (a) Wang, Z.-G.; Hsiao, B. S.; Fu, B. X.; Yeh, F.; Sauer, B. B.; Chang, H.; Schultz, J. M. *Polymer* **2000**, *41*, 1791. (b) Stribeck, N. *Colloid Polym. Sci.* **1993**, *271*, 1007.

(7) Lee, B.; Shin, T. J.; Lee, S. W.; Yoon, J.; Kim, J.; Youn, H. S.; Ree, M. *Polymer* **2003**, *44*, 2509.

(8) Ivanov, D. A.; Amalou, Z.; Magonov, S. N. *Macromolecules* **2001**, *34*, 8944.

(9) Ivanov, D. A.; Pop, T.; Yoon, D. Y.; Jonas, A. M. *Macromolecules* **2002**, *35*, 9813.

(10) Roberts, R. C. *Polym. London* **1969**, *10*, 117.

(11) Bell, J. P.; Murayama, T. *J. Polym. Sci., Part A-2* **1969**, *7*, 1059.

(12) Holdsworth, P. J.; Turner-Jones, A. *Polymer* **1971**, *12*, 195.

(13) Roberts, R. C. *J. Polym. Sci., Polym. Lett.* **1970**, *8*, 381. (c) Jaffee, M.; Wunderlich, B. *Kolloid Z. Z. Polym.* **1967**, *216*, 203. (d) Zachmann, H. G.; Stuart, H. A. *Makromol. Chem.* **1960**, *41*, 148. (e) Sweet, G. E.; Bell, J. P. *J. Polym. Sci., Part A-2* **1972**, *10*, 1273. (f) Alfonso, G. C.; Pedemonte, E.; Ponzetti, L. *Polymer* **1979**, *20*, 104. (g) Groeninckx, G.; Reynaers, H.; Berghmans, H.; Smets, G. *J. Polym. Sci., Polym. Phys. Ed.* **1980**, *18*, 1311. (h) Groeninckx, G.; Reynares, H. *J. Polym. Sci.: Polym. Phys. Ed.* **1980**, *18*, 1325. (i) Fontaine, F.; Ledent, J.; Groeninckx, G.; Reynaers, H. *Polymer* **1982**, *23*, 185. (j) Gehrke, G.; Riekel, C.; Zachmann, H. G. *Polymer* **1989**, *30*, 1582.

(14) Fakirov, S.; Fischer, E. W.; Hoffmann, R.; Schmidt, G. F. *Polymer* **1977**, *18*, 1121.

(15) Medellin-Rodriguez, F. J.; Phillips, P. J.; Lin, J. S.; Campos, R. *J. Polym. Sci.: Polym. Phys.* **1997**, *35*, 1757.

(16) Zhou, Ch.; Clough, S. B. *Polym. Eng. Sci.* **1988**, *28*, 65.

(17) Al Raheil, I. A. M. *Polym. Int.* **1994**, *35*, 189.

(18) Wang, Z.-G.; Hsiao, B. S.; Sauer, B. B.; Kampert, W. G. *Polymer* **1999**, *40*, 4615.

(19) Tan, S.; Su, A.; Li, W.; Zhou, E. *Macromol. Rapid Commun.* **1998**, *19*, 11.

(20) Jonas, A. M.; Russell, T. P.; Yoon, D. Y. *Colloid Polym. Sci.* **1994**, *272*, 1344.

(21) Zachmann, H. G. *Nucl. Instrum. Methods Phys. Res., Sect. B* **1995**, *97*, 209.

(22) Kruger, K. N.; Zachmann, H. G. *Macromolecules* **1993**, *26*, 5202.

(23) Medellin-Rodriguez, F. J.; Phillips, P. J.; Lin, J. S. *Macromolecules* **1996**, *29*, 7491.

(24) Yamadera, R.; Murano, M. *J. Polym. Sci., Part A-1* **1967**, *5*, 2259.

(25) Hachiboshi, M.; Fukuda, T.; Kobayashi, S. *J. Macromol. Sci., Phys.* **1969**, *3*, 525.

(26) Bolze, B.; Kim, J.; Huang, J.-Y.; Rah, S.; Youn, H. S.; Lee, B.; Shin, T. J.; Ree, M. *Macromol. Res.* **2002**, *10*, 2.

(27) Ruland, W. *J. Appl. Crystallogr.* **1971**, *4*, 70.

(28) Koberstein, J. T.; Stein, R. S. *J. Polym. Sci.: Polym. Phys. Ed.* **1983**, *21*, 2181.

(29) Vonk, C. G.; Kortleve, G. *Colloid Polym. Sci.* **1967**, *220*, 19.

(30) Goderis, B.; Reynaers, H.; Koch, M. H. J.; Mathot, V. B. F. *J. Polym. Sci., Phys. Ed.* **1999**, *37*, 1715.

(31) Strobl, G. R.; Schneider, M. *J. Polym. Sci.: Polym. Phys. Ed.* **1980**, *18*, 1343.

(32) Vonk, C. G. *J. Appl. Crystallogr.* **1973**, *6*, 81.

(33) Balta-Calleja, F. J.; Vonk, C. G. *X-ray Scattering of Polymers*; Elsevier: Amsterdam, 1989.

(34) Cheng, S. Z. D.; Cao, M.-Y.; Wunderlich, B. *Macromolecules* **1986**, *19*, 1868.

(35) Marand, H.; Alizadeh, A.; Farmer, R.; Desai, R.; Velikov, V. *Macromolecules* **2000**, *33*, 3392.

(36) (a) Alizadeh, A.; Richardson, L.; Xu, J.; McCartney, S.; Marand, H.; Cheung, Y. W.; Chum, S. *Macromolecules* **1999**, *32*, 6221. (b) Crist, B.; Claudio, E. S. *Macromolecules* **1999**, *32*, 8945.

MA0357321